ACS central science

http://pubs.acs.org/journal/acscii

Research Article

Cytosolic Delivery of Argininosuccinate Synthetase Using a Cell-Permeant Miniature Protein

Susan L. Knox, Rebecca Wissner, Samantha Piszkiewicz, and Alanna Schepartz*

Cite This: *ACS Cent. Sci.* 2021, 7, 641−649

Read Online

ACCESS | Metrics & More | Article Recommendations | Supporting Information

ABSTRACT: Citrullinemia type I (CTLN-I) results from the absence or deficiency of argininosuccinate synthetase (AS), a 46 kDa enzyme that acts in the cytosol of hepatocytes to convert aspartic acid and citrulline into argininosuccinic acid. AS is an essential component of the urea cycle, and its absence or deficiency results in the harmful accumulation of ammonia in blood and cerebrospinal fluid. No disease-modifying treatment of CTLN-I exists. Here we report that the cell-permeant miniature protein (CPMP) ZF5.3 (ZF) can deliver AS to the cytosol of cells in culture and the livers of healthy mice. The fusion protein ZF-AS is catalytically active *in vitro*, stabilized in plasma, and traffics successfully to the cytosol of cultured Saos-2 and SK-HEP-1 cells, achieving cytosolic concentrations greater than 100 nM. This value is 3−10-fold higher than the concentration of endogenous AS (11 ± 1 to 44 ± 5 nM). When injected into healthy C57BL/6 mice, ZF-AS reaches the mouse liver to establish concentrations almost 200 nM above baseline. These studies demonstrate that ZF5.3 can deliver a complex enzyme to the cytosol at therapeutically relevant concentrations and support its application as an improved delivery vehicle for therapeutic proteins that function in the cytosol, including enzyme replacement therapies.

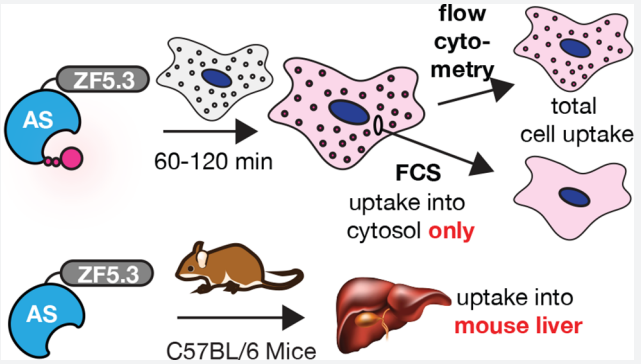

INTRODUCTION

Protein-based drugs represent the fastest growing segment of the modern-day pharmacopeia. More than one-quarter of all new drugs approved over the past three years are biologics.[1] These new molecular entities—which include antibodies, antibody−drug conjugates, cytokines, fusion proteins, growth factors, and enzymes—treat diseases ranging from lymphomas to macular degeneration to asthma, and are projected to account for 35% of the global pharmaceutical revenue by 2025.[2,3] Yet despite this enormous impact on human health, the full potential of protein therapeutics cannot yet be realized for one simple reason: most exogenous proteins cannot reach the cell interior—the cytosol. This singular limitation hinders the development of protein therapeutics that replace, inhibit, or activate therapeutic targets within the cytosol, nucleus, or interior organelles. Although it has been 30 years since the first reports of cell penetration by the HIV protein known as Tat,[4,5] the reality is that most large, proteinaceous materials are taken up by cells into the endocytic pathway, and within the endocytic pathway they remain.[6,7] There is little question that a more complete understanding of the mechanisms and structure-activity relationships that allow certain large protein aceous materials to escape endosomes would accelerate the design of next-generation protein therapeutics that target the large fraction of the proteome that remains undruggable.[8]

The enormous interest in protein delivery has led to multiple reports of peptide-based materials capable of "endosomal escape".[6,7] Unfortunately, few of these reports compare different delivery vehicles under identical conditions and in a manner that allows a direct and quantitative assessment of how much material reaches the cytosol.[9] Fewer still evaluate whether the material that reaches the cytosol remains intact. Recently it was reported that the cell-permeant miniature protein (CPMP) ZF5.3 (ZF) traffics with unprecedented efficiency to the cytosol and nucleus without cytotoxic effects,[8,10,11] even when fused to protein cargo.[9] A head-to-head comparison of seven putative cell-penetrating peptides (CPPs), macrocycles,[12] and CPMPs as delivery vehicles for the model cargo SNAP-tag (188 aa, 20 kDa) established that the CPMP ZF5.3[8,10,11] could deliver SNAP-tag to the cytosol at concentrations 2- to 9-fold higher than any other vehicle tested.[9] Subsequent work showed that the efficacy of ZF5.3 as a delivery vehicle may be related to a previously unrecognized portal for endosomal escape that demands the homotypic fusion and vacuole protein sorting (HOPS) complex, an essential component of the endocytic

Received: November 27, 2020
Published: March 18, 2021

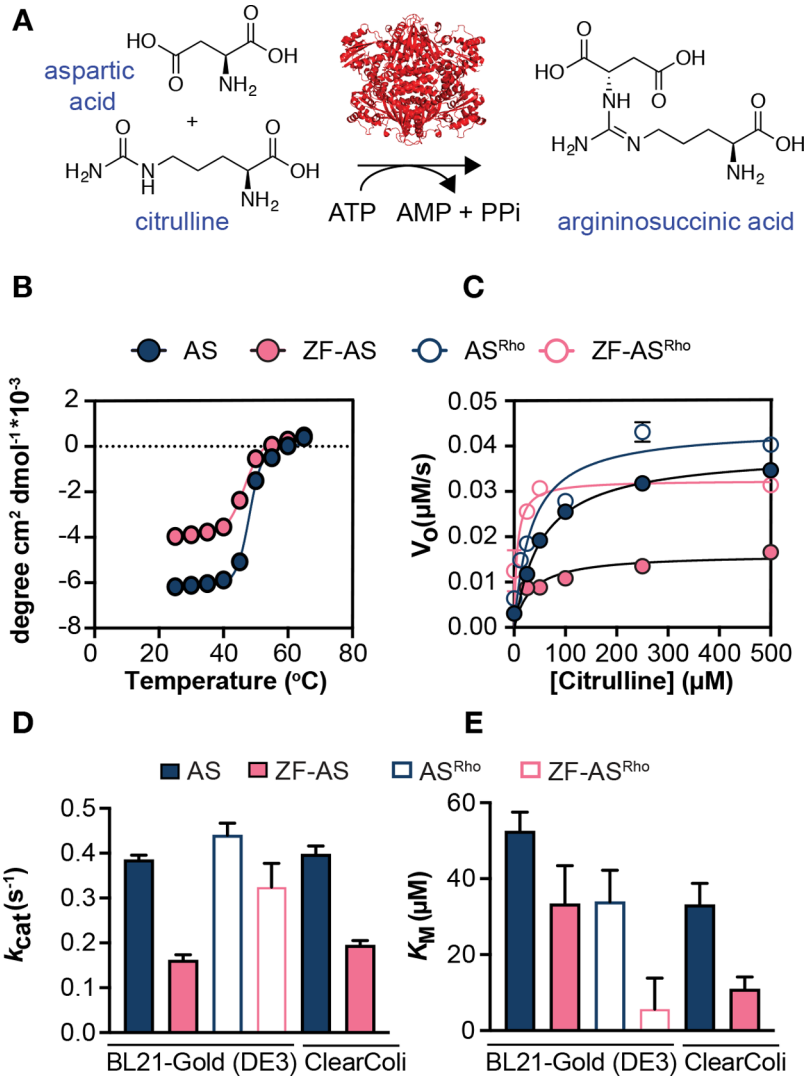

Figure 1. (A) Argininosuccinate synthetase (AS) catalyzes the conversion of aspartic acid and citrulline into argininosuccinic acid during the first cytosolic step of the urea cycle. (B) Graphs illustrating the change in molar ellipticity at 222 nm of AS and ZF-AS as a function of temperature. The apparent T_M of each protein (48.1 °C for AS and 46.6 °C for ZF-AS) was determined by fitting the melting curve to a Boltzmann sigmoidal curve in Prism (Version 8.4.3); the melts were not reversible. (C) Plot illustrating the initial velocity (V_o) of NADH production (as determined by the absorbance at 340 nm) as a function of citrulline concentration (0−500 μM) in reactions containing 100 nM AS, ZF-AS, AS^{Rho}, or ZF-AS^{Rho} (all expressed in BL21-Gold (DE3)). (D) Bar graph showing k_{cat} values for AS, ZF-AS, AS^{Rho}, and ZF-AS^{Rho}, as determined from the best fit of the initial velocity data to the Michaelis−Menten equation (expressed in either BL21-Gold (DE3) for biochemical analyses or ClearColi for mouse studies). (E) Bar graph representing K_M values of AS, ZF-AS, AS^{Rho}, and ZF-AS^{Rho} with respect to citrulline (expressed in either BL21-Gold (DE3) for biochemical analyses or ClearColi for mouse studies). V_o plots were fit to a standard Michaelis−Menten equation using Prism (Version 8.4.3). For the V_o plots, error bars represent the standard error. Error bars in the k_{cat} and K_M bar graphs represent the standard error of the mean.

machinery.[8] These studies provide evidence that ZF5.3-enzyme fusions can escape endosomes with unprecedented efficiency and suggest that they do so via a defined and underexploited mechanism. Here we ask whether ZF5.3 can deliver a therapeutically relevant cargo, a complex, multimeric enzyme that is lost or mutated in patients with citrullinemia type 1 (CTLN-1).

The metabolic disorder CTLN-I results from loss or depletion of argininosuccinate synthetase (AS), a tetrameric enzyme that converts citrulline and aspartic acid to argininosuccinic acid within the cytosol of hepatocytes (Figure 1A).[13] AS is an essential component of the urea cycle, and its absence or deficiency blocks the conversion of ammonia, a byproduct of amino acid catabolism, into urea.[14] Without AS, ammonia accumulates in blood and cerebrospinal fluid, resulting in multiple neurological effects that include permanent brain damage.[15] Current treatments for CTLN-I include diet control, nitrogen scavenger therapy, hemodialysis, and liver transplantation, but all are symptomatic—none of these treatments target the underlying cause of disease.[15] Enzyme replacement therapy would provide a disease-modifying alternative to current symptomatic treatments with the potential to significantly improve patient quality of life. Previous studies have described the delivery of adeno-associated virus (AAV) vectors encoding AS to mice and extracellular vesicles (EVs) containing AS to hepatocytes.[16,17] Although these approaches highlight the feasibility of AS enzyme replacement therapy, obstacles remain that hamper their implementation as therapeutics.[18−24] We hypothesized that fusion of the CPMP ZF5.3 to AS would generate a new

https://doi.org/10.1021/acscentsci.0c01603
ACS Cent. Sci. 2021, 7, 641−649

bifunctional protein with improved ability to traffic directly into the cell cytosol, an essential first step in circumnavigating concerns with delivery via AAV vectors and EVs.

Here we show that ZF-AS, a fusion protein containing both ZF5.3 and AS, retains the ability to oligomerize, is catalytically active *in vitro*, and resists rapid proteolysis in plasma. Quantitative analysis of intracellular trafficking using fluorescence correlation spectroscopy[11,25] reveals that ZF-AS reaches the cytosol of Saos-2 and SK-HEP-1 cells to achieve concentrations as high as 111 ± 19 nM; this range is 3−10-fold higher than the endogenous concentration of AS in mouse liver homogenate (11 ± 1 to 44 ± 5 nM). When injected into healthy C57BL/6 mice, ZF-AS reaches the mouse liver to achieve concentrations almost 200 nM above baseline. These studies provide proof-of-concept that the CPMP ZF5.3[8−11] can deliver a complex, multimeric enzyme to the cytosol of cultured cells and internal mouse organs.

RESULTS AND DISCUSSION

Expression, Purification, and Characterization of AS and ZF-AS. Our first task was to prepare samples of AS and ZF-AS that were suitable for both *in vitro* analysis of enzyme activity and plasma stability as well as the optimization of enzyme-linked immunosorbent (ELISA) assays to detect these materials within serum and liver. The sequence encoding human AS (411 aa, 46.5 kDa) and its N-terminal fusion with ZF (27 aa, 3.2 kDa) were cloned into a pET-32a expression vector downstream of a His_6-SUMO tag, overexpressed in BL21-Gold (DE3) competent *E. coli*, and purified by immobilized metal affinity chromatography (IMAC). The SUMO-tag was subsequently removed using SUMO protease,[26] and the final materials were purified to ≥90% homogeneity using size exclusion chromatography (SEC) (Figure S1A and B). Protein identities were confirmed by LC/MS (Figure S1C). When analyzed by high-resolution preparative gel filtration, AS coeluted with phosphorylase B (97.2 kDa) and aldolase (158 kDa) standards (Figure S1D). ZF-AS eluted slightly earlier than AS and aldolase, suggesting that both AS and ZF-AS assemble predominantly into tetramers in the micromolar concentration range and that the fusion of ZF to the AS N-terminus did not measurably alter the tetramer equilibrium dissociation constant (Figure S1D).[27]

We next assessed whether ZF-AS could recapitulate the essential biochemical and biophysical metrics associated with AS. Although point mutations near the AS active site (such as A118T and T119I) lead to moderate (<5 °C) decreases in thermal stability (T_M) as assessed by differential scanning fluorimetry (wild-type T_M = 49 °C),[28] no reports describe the effects of N- or C-terminal fusions on thermal stability. The apparent T_M of purified AS determined by circular dichroism (CD) spectroscopy (48.1 °C) was in line with previous reports (49 °C)[28] and only moderately higher than the value determined for ZF-AS (46.6 °C) under identical conditions (Figure 1B). Although the melting transitions of both AS and ZF-AS were irreversible, their premelt wavelength-dependent CD spectra were virtually identical and consistent with significant α-helical secondary structure, as expected (Figure S1E). The time-dependent proteolytic stabilities of AS and ZF-AS in mouse plasma were also virtually identical, with close to 70% fully intact protein remaining after 6 h (Figure S2).

Samples of AS^{Rho} and ZF-AS^{Rho} used for confocal microscopy, flow cytometry, and FCS were prepared in a three-step process. AS and ZF-AS were first expressed as fusion proteins containing both a N-terminal His_6-SUMO tag and a C-terminal LPETGG tag; these materials were then subjected to a sortase-catalyzed transpeptidation reaction[29−31] with $GGGK^{Rho}$, a tetrapeptide containing Lissamine rhodamine B (Rho) at the C-terminus. To streamline the synthesis, we designed a one-pot reaction to simultaneously remove the His_6-SUMO tag and append $GGGK^{Rho}$ (Figure S3A) to produce AS^{Rho} and ZF-AS^{Rho}. Reaction duration, temperature, and buffer composition were varied to optimize yield and purity (Figure S4); we found that dialyzing SUMO protease, sortase, and AS or ZF-AS into the same HEPES-containing buffer at pH 7 prior to the one-pot reaction resulted in the highest yield of labeled and purified product. Final materials were purified by SEC and analyzed by electrospray mass spectrometry (Figure S3B and C).

ZF-AS fusion proteins are catalytically active. Argininosuccinate synthetase (AS) plays a critical role in the segment of primary metabolism known as the urea cycle, which eliminates excess nitrogen through the combined action of six enzymes and two mitochondrial transporters.[32] As the third enzyme in this pathway, AS converts aspartic acid, citrulline, and ATP into argininosuccinic acid.[32] The two-step enzymatic reaction leads ultimately to the release of argininosuccinic acid, PP_i, and AMP (Figure 1A) and can be followed spectrophotometrically by monitoring the release of either pyrophosphate or AMP.[33] Historically, AS activity has been quantified using a discontinuous assay that monitors urea production[34] or citrulline utilization,[35] or continuously by monitoring the pyrophosphate-dependent oxidation of nicotinamide adenine dinucleotide (NADH).[36] While PP_i is a byproduct of the initial AS-catalyzed activation of aspartic acid, AMP release occurs only upon formation of the final product argininosuccinic acid. Thus, we chose to monitor release of AMP by coupling its production to NADH oxidation in a well-validated enzyme-linked assay that uses myokinase to convert AMP to ADP (Figure S5).[37] The catalytic constants determined in this way are summarized in Table S2.

First we sought to compare the catalytic constants of recombinant AS and ZF-AS to previously determined values for AS isolated from *E. coli* and human or bovine liver.[15,33,38−42] Reported values of k_{cat} for AS vary from <0.1 to 1 s^{-1},[33,38,39,41,42] while K_M values range from 0.01 to 112 μM.[33,39−43] The catalytic constants determined for human AS purified from BL21-Gold (DE3) cells fell within this range, with k_{cat} and K_M values of 0.39 ± 0.01 s^{-1} and 52 ± 5 μM, respectively (Figure 1C−E, Figure S5E). The catalytic constants determined for ZF-AS also fell in this range, with respect to both k_{cat} (0.16 ± 0.01 s^{-1}) and K_M (33 ± 10 μM), although we note that the k_{cat} measured for ZF-AS is 2.4-fold lower than that of AS. Heat denaturation of AS and ZF-AS at 95 °C led to completely inactive enzymes, with no significant time-dependent change in absorbance at 340 nm for either sample (Figure S5F). The kinetic constants of AS^{Rho} and ZF-AS^{Rho} also fell within the expected ranges, with k_{cat} values of 0.44 ± 0.02 s^{-1} and 0.32 ± 0.05 s^{-1} and K_M values of 34 ± 8 μM and 6 ± 8 μM, respectively, for AS^{Rho} and ZF-AS^{Rho}. Although the AS C-terminus participates in hydrophobic interactions and a single salt bridge within the tetrameric complex visualized by crystallography,[27] the uniformity of the kinetic constants determined for ZF-AS, AS^{Rho}, and ZF-AS^{Rho} indicate that the enzyme tolerates the addition of ZF to the N-terminus and the addition of a $LPETGGGK^{Rho}$ tag to the C-terminus. Overall, these studies provide confidence that both

https://doi.org/10.1021/acscentsci.0c01603
ACS Cent. Sci. 2021, 7, 641−649

ZF-AS and ZF-AS^{Rho} can process aspartic acid and citrulline into argininosuccinic acid *in vitro*. In addition to the activity studies described here, we confirmed that ZF-AS and AS displayed comparable catalytic activities when spiked into a liver homogenate (Figure S6).

Evaluation of Uptake by Saos-2 Cells Using Flow Cytometry and Confocal Microscopy. With purified, catalytically active, Rho-labeled materials in hand, we turned to confocal microscopy and flow cytometry to assess the relative overall uptake of ZF-AS^{Rho} and AS^{Rho} by Saos-2 cells. Saos-2 cells were chosen because they are well-suited for subsequent analysis of cytosolic and/or nuclear uptake using fluorescence correlation spectroscopy (FCS).[25] Briefly, cells were treated for 1 h with 1−3 μM purified ZF-AS^{Rho} or AS^{Rho}, washed, treated with trypsin to eliminate cell surface-bound material, imaged using confocal microscopy (Figure 2A and B), and assayed *en masse via* flow cytometry (Figure 2C and D). When visualized using confocal microscopy, intact Saos-2 cells show clear evidence of punctate rhodamine fluorescence when treated with increasing concentrations of ZF-AS^{Rho} (Figure S7), whereas little punctate fluorescence is observed in cells treated with AS^{Rho} (Figure 2B and Figure S7). The difference in overall uptake is more evident when ZF-AS^{Rho}- and AS^{Rho}-treated Saos-2 cells are evaluated *en masse* using flow cytometry (Figure 2C and D). The median fluorescence intensity (MFI) of Saos-2 cells treated with AS^{Rho} increases moderately if at all (1.6-fold) as the incubation concentration increases from 1 to 3 μM, while the MFI of Saos-2 cells treated with ZF-AS^{Rho} increases 7.4-fold over the same concentration range. Overall, treatment of Saos-2 cells for 1 h with ZF-AS^{Rho} resulted in higher MFI values than observed when cells were treated with ZF-SNAP^{Rho} at all concentrations (1−3 μM) and time points (0.5 and 2 h).[9] It is possible that the higher overall uptake of ZF-AS^{Rho} relative to ZF-SNAP^{Rho} is related to differences in overall charge that affect association with the plasma membrane.[44−46]

Evaluation of Cytosolic Trafficking of AS^{Rho} and ZF-AS^{Rho} Using Fluorescence Correlation Spectroscopy (FCS). After assessing cellular uptake by confocal microscopy and flow cytometry, we used FCS[8,9,25] to track the concentration-dependent endosomal release of ZF-AS^{Rho} and AS^{Rho} into the cytosol of Saos-2 cells (Figure 2E and Figure S8). These experiments revealed that treatment of Saos-2 cells with 1 to 3 μM ZF-AS^{Rho} leads to cytosolic ZF-AS^{Rho} concentrations between 35 ± 4 nM and 111 ± 19 nM after 1 h. ZF-AS^{Rho} achieves the highest cytosolic concentration at 2 μM; the minimal differences between 2 μM and 3 μM may illustrate saturation of the cellular mechanism required for endosomal release.[8] By contrast, the cytosolic concentrations achieved by AS^{Rho} fell between 26 ± 6 nM and 77 ± 30 nM and were not dose-dependent. The largest difference in cytosolic concentrations achieved by AS^{Rho} and ZF-AS^{Rho} (4-fold) was observed at an incubation concentration of 3 μM. It is notable that the cytosolic concentrations achieved by ZF-AS^{Rho} are lower than previously observed for ZF-SNAP^{Rho}, even at shorter incubation times.[9] This difference may reflect the fact that ZF-AS^{Rho} is a tetramer of 49.9 kDa monomers and ZF-SNAP^{Rho} is a monomer (23.3 kDa). Cytosolic fractionation experiments confirmed that ZF-AS^{Rho} remains intact when delivered to the cytosol of Saos-2 cells (Figure S9).

We also assessed whether cytosolic delivery of ZF-AS^{Rho} demanded a covalent linkage between AS and ZF5.3. Specifically, we evaluated whether ZF5.3 (unadorned by a fluorescent tag) would increase the ability of AS^{Rho} to (1) localize within the endosomal pathway ("uptake") and (2) reach the cytosol ("endosomal release"). Saos-2 cells were

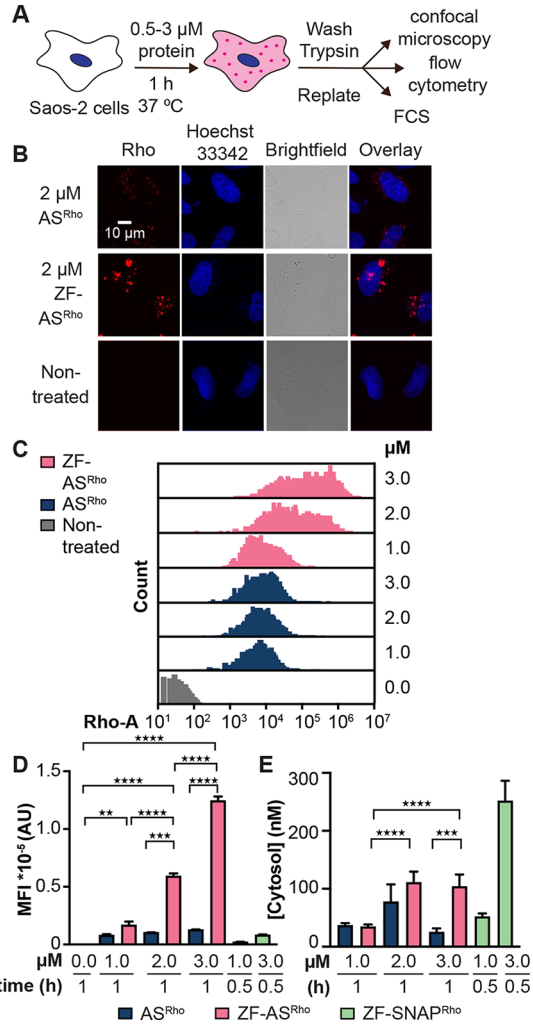

Figure 2. (A) Scheme illustrating confocal microscopy, flow cytometry, and fluorescence correlation spectroscopy (FCS) workflow. Saos-2 cells were treated with 1−3 μM of AS^{Rho} or ZF-AS^{Rho} for 1 h. Cells were washed, treated with trypsin, and either screened using flow cytometry or replated and imaged using confocal microscopy and FCS. (B) Total cellular uptake of AS^{Rho} and ZF-AS^{Rho} assessed using confocal microscopy. Live cell images of Saos-2 cells treated with 2 μM of the indicated protein for 1 h. Scale bar = 10 μm. (C) Histograms and (D) bar plots illustrating total cellular uptake of 1−3 μM AS^{Rho} or ZF-AS^{Rho} during a 1 h incubation at 37 °C. Data for ZF-SNAP^{Rho} were previously published.[9] MFI values represent the median fluorescence intensity of cells (10,000 cells each). Error bars represent the standard error of the mean. The MFI values of AS^{Rho} at each concentration (1−3 μM) were statistically compared to the MFI values of ZF-AS^{Rho} at each concentration (1−3 μM). ****$p \leq 0.0001$, ***$p \leq 0.001$, **$p \leq 0.01$, *$p \leq 0.05$; one-way analysis of variance (ANOVA) followed by Tukey's multiple comparisons test. (E) Cytosolic access of AS^{Rho} and ZF-AS^{Rho} assessed using fluorescence correlation spectroscopy. Bar plot illustrating the cytosolic concentrations achieved in Saos-2 cells after a 1 h incubation with 1−3 μM of AS^{Rho} and ZF-AS^{Rho}. The average intracellular concentrations of each AS^{Rho} treatment condition (1−3 μM) were statistically compared to the average intracellular concentration of each ZF-AS^{Rho} treatment condition (1−3 μM) using an one-way ANOVA followed by Sidak's multiple comparisons test. ****$p \leq 0.0001$, ***$p \leq 0.001$, **$p \leq 0.01$, *$p \leq 0.05$.

https://doi.org/10.1021/acscentsci.0c01603
ACS Cent. Sci. 2021, 7, 641−649

incubated for 1 h with 1 μM AS^{Rho} plus 0−1 μM ZF5.3; the total cellular uptake of AS^{Rho} was determined by flow cytometry, and the concentration of AS^{Rho} in the cytosol was determined using FCS (Figure S10A). Increasing amounts of ZF5.3 led to a dose-dependent increase in the total cellular uptake of AS^{Rho} (Figure S10B) but no change in the amount of AS^{Rho} that reaches the cytosol (Figure S10C). These results confirm that efficient cytosolic delivery of ZF-AS demands a covalent linkage between AS and ZF5.3, and are fully consistent with the previous observation that ZF5.3 does not increase the amount of Lys9^{Rho} that reaches the cytosol when cells are incubated with both compounds.[8]

Evaluation of Uptake by SK-HEP-1 Cells Using Flow Cytometry and Confocal Microscopy. Next we turned to SK-HEP-1 cells, human hepatic adenocarcinoma cells that naturally express low levels of AS, providing a disease-relevant system.[47] SK-HEP-1 cells were treated with between 0.5 and 3 μM ZF-AS^{Rho} or AS^{Rho} for 1 or 2 h, washed, treated with trypsin, and evaluated using confocal microscopy, flow cytometry, and FCS (Figure 3, Figure S11, Figure S12A and B). Cells treated with AS^{Rho} show no increase in punctate fluorescence with incubation time but a minimal increase with respect to concentration (Figure S11). By contrast, ZF-AS^{Rho} showed both time- and dose-dependent increases in punctate fluorescence (Figure S11). The median fluorescence intensity (MFI) of cells treated with 0.5 to 3 μM AS^{Rho} increased moderately from 4540 ± 50 to 6860 ± 110 AU over this concentration range, whereas the MFI of cells treated with analogous concentrations of ZF-AS^{Rho} exhibited dose dependency and increased from 11 000 ± 1000 AU to a maximum of 38 000 ± 2000 AU (Figure 3C and E). The decrease in overall uptake at 3 μM could be the result of cell death (Figure S12C). The overall uptake of both AS^{Rho} and ZF-AS^{Rho} was also time-dependent, as observed previously,[9] with higher uptake observed at longer incubation times (Figure 3E).

Evaluation of Cytosolic Trafficking of AS^{Rho} and ZF-AS^{Rho} in SK-HEP-1 Cells Using FCS. After assessing overall cellular uptake by confocal microscopy and flow cytometry, we used FCS[8,9,25] to track the endosomal release of ZF-AS^{Rho} and AS^{Rho} by monitoring the concentration of each protein within the SK-HEP-1 cytosol as a function of dose (1−3 μM) and time (1−2 h) (Figure 3A and Figure S12D). These experiments revealed several important observations. First, the FCS data revealed that AS^{Rho} itself reaches the SK-HEP-1 cytosol more efficiently than previously studied proteins lacking ZF.[9] The concentration of AS^{Rho} in the cytosol averages 47 ± 6 nM, which is 24-fold larger than that achieved by SNAP-tag^{Rho} under comparable conditions (2 ± 1 nM in Saos-2 cells) despite the difference in molecular mass.[9] Importantly, the amount of AS^{Rho} that traffics into the cytosol is independent of both dose (0.5−3 μM) and incubation time (1−2 h). Second, the improvements in cytosolic trafficking of AS due to ZF (no significant differences at 2 and 3 μM) are smaller than previously observed for the model protein SNAP-tag (approximately 2.3-fold at 2 and 3 μM).[9] At lower concentrations the dose−response was nonlinear, with maximal cytosolic concentrations of ZF-AS^{Rho} observed at 1 μM with a 1 h incubation (Figure 3F). ZF-AS^{Rho} reaches the SK-HEP-1 cytosol at concentrations greater than 50 μM under all experimental conditions, whereas a 3 μM dose is required for AS^{Rho} to reach this threshold. A final observation is that there are subtle cell line-dependent differences; in Saos-2 cells, an incubation concentration of 2 μM led to the highest

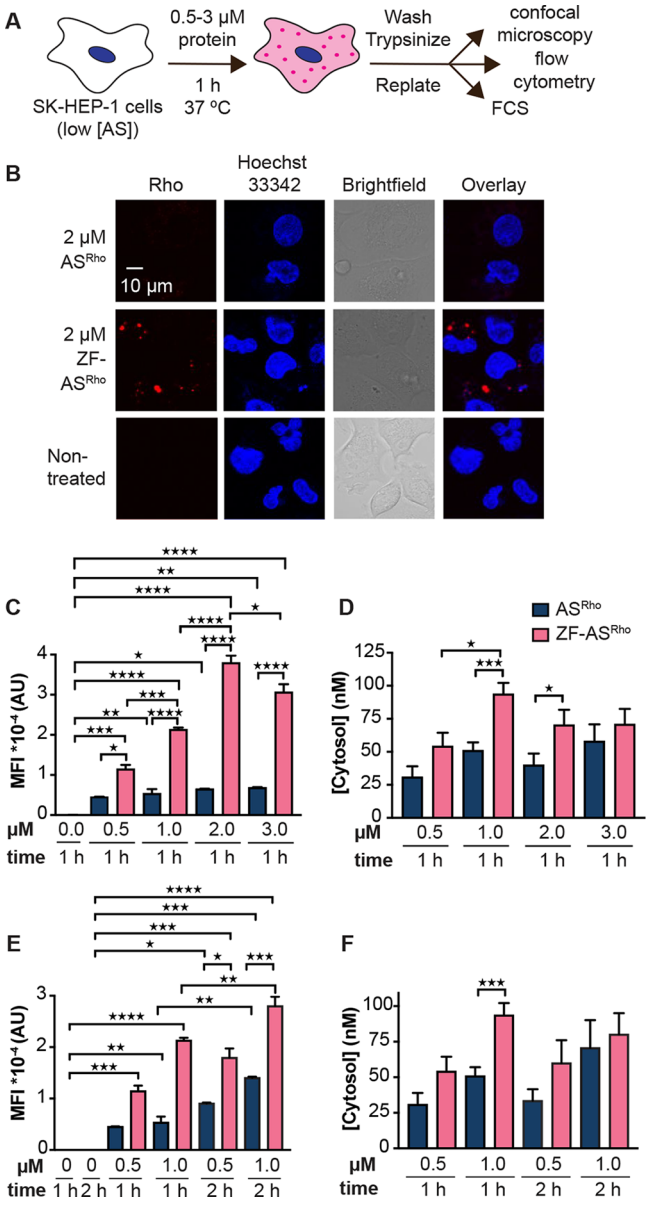

Figure 3. (A) Scheme of confocal microscopy, flow cytometry, and fluorescence correlation spectroscopy (FCS) experiments. SK-HEP-1 cells were treated with 0.5−3 μM of AS^{Rho} or ZF-AS^{Rho} for 1 or 2 h. Cells were washed, trypsinized, and either used for flow cytometry or replated and evaluated by confocal microscopy and FCS. (B) Total cell uptake of AS^{Rho} and ZF-AS^{Rho} assessed by confocal microscopy. Live cell images of SK-HEP-1 cells treated with 2 μM of protein for 1 h. Scale bar = 10 μm. (C) Bar plots illustrating total cellular uptake of AS^{Rho} and ZF-AS^{Rho} at 0.5−3 μM during a 1 h incubation. MFI values represent the median fluorescence intensity of cells (10,000 cells each). Error bars represent the standard error of the mean. The MFI values of AS^{Rho} at each concentration (0.5−3 μM) were statistically compared to the MFI values of ZF-AS^{Rho} at each concentration (0.5−3 μM). ****$p \le 0.0001$, ***$p \le 0.001$, **$p \le 0.01$, *$p \le 0.05$; one-way analysis of variance (ANOVA) followed by Tukey's multiple comparisons test. (D) Bar plot of cytosolic concentrations in SK-HEP-1 cells with a 1 h treatment of 0.5−3 μM of AS^{Rho} or ZF-AS^{Rho}. The average intracellular concentrations achieved with each AS^{Rho} treatment condition (0.5−3 μM) were statistically compared to the average intracellular concentration achieved with each ZF-AS^{Rho} treatment condition (0.5−3 μM) using an unpaired t test, two-tailed. ****$p \le 0.0001$, ***$p \le 0.001$, **$p \le 0.01$, *$p \le 0.05$. (E) Bar plots illustrating total cellular uptake of AS^{Rho} and ZF-AS^{Rho} at 0.5−1 μM

https://doi.org/10.1021/acscentsci.0c01603
ACS Cent. Sci. 2021, 7, 641−649

Figure 3. continued

during a 1 or 2 h incubation. MFI values represent the median fluorescence intensity of cells (10,000 cells each). Error bars represent the standard error of the mean. MFI values corresponding to each AS conjugate were statistically compared to all other protein samples. ****$p \leq 0.0001$, ***$p \leq 0.001$, **$p \leq 0.01$, *$p \leq 0.05$; one-way analysis of variance (ANOVA) followed by Tukey's multiple comparisons test. (F) Bar plot of the cytosolic concentrations measured in SK-HEP-1 cells after a 1 or 2 h treatment with 0.5−1 μM AS^{Rho} or ZF-AS^{Rho}. The average intracellular concentration of AS^{Rho} after each treatment condition (0.5−1 μM, 1 or 2 h) was statistically compared to the average intracellular concentration of ZF-AS^{Rho} after the same treatment condition (0.5−3 μM) using an unpaired t test, two-tailed. ****$p \leq 0.0001$, ***$p \leq 0.001$, **$p \leq 0.01$, *$p \leq 0.05$.

cytosolic concentration of ZF-AS^{Rho}, whereas only a 1 μM dose was required to reach this concentration in SK-HEP-1 cells. Taken together, these data indicate that ZF can transport AS into the cytosol of multiple cell lines to achieve concentrations that approximate that of endogenous AS in a healthy C57BL/6 mouse liver (Figure S13). We note that the presence of Zn^{2+} is essential for delivery of ZF-AS: when prepared in the absence of Zn^{2+}, the concentration of ZF-AS^{Rho} that reaches the cytosol falls to the level achieved by AS^{Rho} alone (Figure S12E and F). This finding is consistent with previous reports that disruption of the α-helix in aPP5.3 also lowers delivery efficiency.[48]

Endotoxin Analysis and Removal. The outer membrane of Gram-negative bacteria such as *E. coli* is replete with lipopolysaccharides (LPS) known as endotoxins.[49] LPS is released from lysed bacteria[50] and can copurify with proteins isolated from *E. coli*.[51,52] Interaction of the hexa-acyl chain of LPS with Toll-like receptor 4 (TLR4) in complex with myeloid differentiation factor 2 (MD-2) activates the innate immune response in mammalian cells and can cause myriad detrimental effects, including a cytokine storm.[53−56] Indeed, AS has been reported to itself bind LPS.[13,57] Our experiments necessitated that endotoxin levels be reduced to less than five endotoxin units (EU) per kilogram of mouse (1 EU/mL protein) prior to animal studies.[58−60] We initially quantified endotoxin levels using a *Limulus* amebocyte lysate (LAL), which exploits the endotoxin binding activity of Factor C in the innate immune response of horseshoe crabs.[61] Using the LAL assay, we quantified the level of endotoxin contamination in samples of AS and ZF-AS isolated from BL21-Gold (DE3) cells (Figure S14A−C). This assay revealed endotoxin levels of 9.3 ± 1.1 EU/mL (AS) and 9.6 ± 0.3 EU/mL (ZF-AS), significantly higher than those in Milli-Q water and buffer (0.068 ± 0.001 and 0.067 ± 0.000 EU/mL, respectively), limiting the potential dose in a mouse study to <1 μM (0.25 mg/kg).

We made use of the engineered BL21(DE3) *E. coli* strain ClearColi and extensive wash steps to reduce the endotoxin contamination of AS and ZF-AS in preparation for animal studies (Figure 4A). ClearColi lacks multiple genes required for lipid A biosynthesis (Δ*gutQ*, Δ*kdsD*, Δ*lpxL*, Δ*lpxM*, Δ*pagP*, Δ*lpxP*, and Δ*etpA*).[53,62] To evaluate the level of endotoxin contamination in materials generated in ClearColi, we used an engineered HEK293 cell line (HEK-Blue hTLR4, InvivoGen) that reports on the direct interaction of endotoxin with TLR4 and MD-2 with a chromophore that is monitored at 640 nm (Figure 4B).[55,56,63,64] We first assessed the endotoxin levels of the SUMO protease used during the workflow used to prepare AS and ZF-AS (Figure 4C). The endotoxin levels in the SUMO protease samples decreased

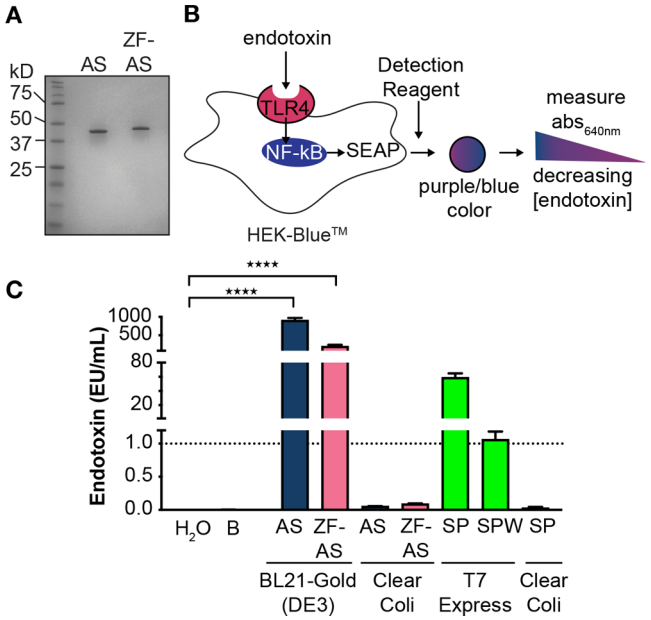

Figure 4. (A) SDS-PAGE analysis illustrating final purity of AS and ZF-AS produced in ClearColi cells and used for *in vivo* mouse study. The final purity of both AS and ZF-AS was >99%. (B) Experimental scheme illustrating the HEK-Blue cell-based assay, which monitors the binding of endotoxin to the TLR4 receptor and activates downstream cellular signals (NF-κB production). When NF-κB is activated, a secreted embryonic alkaline phosphatase (SEAP) is produced and secreted into the media. The absorbance of a proprietary SEAP detection reagent is monitored at 640 nm. (C) Endotoxin levels (EU/mL) as determined from the HEK-Blue hTLR4 response with HEK-Blue Detection. The HEK-Blue hTLR4 assay measures the interaction of the hexa-acyl chain of endotoxin (and can distinguish the modified ClearColi acyl chain). The buffer (denoted as B) was 30 mM HEPES (pH 7.5), 500 mM NaCl, and 10% glycerol. SUMO protease purified from the T7 Express *E. coli* strain with an initial 30−40 CV 0.1% Triton X-114 wash during the IMAC step (Figure S1A) is denoted as SP, SUMO protease further purified with an additional 88 CV 0.1% Triton X-114 wash during the IMAC step is denoted as SPW, and SUMO protease purified from ClearColi is denoted as SP. Error is standard error of the mean. The average endotoxin level of Milli-Q water was statistically compared to the average endotoxin level of each protein sample using a one-way ANOVA followed by Dunnett's multiple comparisons test. ****$p \leq 0.0001$, ***$p \leq 0.001$, **$p \leq 0.01$, *$p \leq 0.05$.

from 59 ± 6 EU/mL for material expressed in BL21-Gold (DE3) cells to 0.03 ± 0.02 EU/mL for material produced in ClearColi, a 2000-fold reduction. In T7 Express cells, just an additional wash step decreased endotoxin levels almost 60-fold.

We next assessed the levels of endotoxin contamination in samples of AS and ZF-AS expressed in different *E. coli* strains (Figure 4C). Expression of AS and ZF-AS in ClearColi led to endotoxin levels that were reduced by 16 500-fold (AS) or 2000-fold (ZF-AS) from levels observed for samples expressed in BL21-Gold (DE3) cells. The level of endotoxin contamination in the final ZF-AS sample (0.091 ± 0.006 EU/mL) was suitable to allow mouse dosing at 3 mg/kg. The ClearColi-derived proteins AS and ZF-AS exhibited k_{cat} values (0.40 ± 0.02 s^{-1} and 0.19 ± 0.01 s^{-1}, respectively) similar to those for the enzymes purified from BL21-Gold (DE3) cells (Figure 1D). The K_M values of ClearColi purified proteins did slightly decrease by 1.6- and 3-fold compared to AS and ZF-AS

https://doi.org/10.1021/acscentsci.0c01603
ACS Cent. Sci. 2021, 7, 641−649

purified from BL21-Gold (DE3) cells, respectively (Figure 1E).

Delivery to Healthy Mice. With endotoxin-free material in hand, we next asked whether ZF-AS purified from ClearColi would reach the liver of C57BL/6 mice when administered *in vivo*. A set of 30 C57BL/6 mice were injected intravenously via the tail vein with 3 mg/kg ZF-AS (15 mice) or vehicle (phosphate buffered saline (pH 7.4)) (15 mice), and the time-dependent concentrations of AS-containing proteins in serum and liver were evaluated using organ-specific ELISAs detecting an internal AS epitope (Figure 5). These assays were optimized

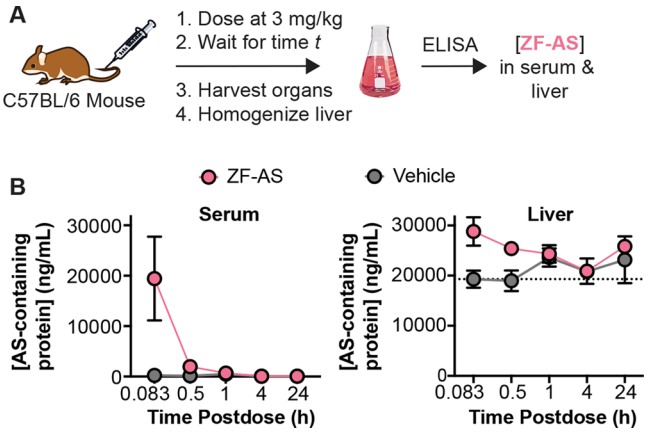

Figure 5. (A) Scheme for dosing of ZF-AS into C57BL/6 mice. Mice were injected with either 3 mg/kg ZF-AS (in DPBS) or vehicle (DPBS) into the tail vein. Three mice were sacrificed at each time point (0.083, 0.5, 1, 4, 24 h), their organs were harvested, blood was processed to serum, and liver was processed to homogenate. The concentration of ZF-AS present in serum and liver samples was evaluated using an enzyme-linked immunosorbent assay (ELISA). (B) Concentration of AS-containing proteins detected in serum or liver over time.

to quantify dilutions of ZF-AS at concentrations between 1.6 and 200 nM (in serum) and 0.1 and 6.0 nM (in liver) (Figure S15). Mice injected with 3 mg/kg ZF-AS showed a total ZF-AS concentration in serum of 390 ± 1706 nM (19400 ± 8300 ng/mL) above baseline (vehicle signal) within the first 5 min of dosing. The rapid loss of ZF-AS from serum observed here is consistent with the previous observation that intravenous injection of 0.11−0.43 mg/kg rat-liver purified AS remains in serum for less than 15 min postdose.[65] Mice injected with vehicle alone showed an initial liver concentration of AS-containing protein of roughly 410 ± 40 nM (19300 ± 1700 ng/mL), which was defined as baseline. We note that this value does not rigorously reflect the concentration of endogenous AS in the liver as the ELISA was optimized to quantify ZF-AS, not AS. Mice injected with 3 mg/kg ZF-AS showed a total ZF-AS concentration in the liver of 190 ± 60 nM above baseline at short times; this value decreased to baseline values over the course of 1 h. Although the rapid clearance of ZF-AS from the liver is not ideal, this initial study shows definitively that ZF-AS is nontoxic to mice at 3 mg/kg, is stable in plasma, and reaches the liver at concentrations close to 200 nM within 1 h of dosing. Experiments to assess the efficacy of ZF-AS versus AS in an established mouse model for CTLN-I (*Ass1*^{fold}-mice)[66] will be described in due course.

CONCLUSIONS

Previous work has provided evidence that a fusion of the cell-permeant miniature protein (CPMP) ZF5.3 (ZF) with the small model protein SNAP-tag can enter cells and escape from endosomes with greater efficiency than fusions to either canonical (penetratin) or macrocyclic (CPP9 and CPP12)[12] delivery vehicles.[9] Indeed, cytosolic delivery of SNAP-tag using the macrocycles CPP9 or CPP12 was virtually undetectable, even at high concentrations and extended times.[9] Here we report that ZF is also capable of delivering a large and complex urea cycle enzyme, argininosuccinate synthetase, to the cytosol of cells in culture and the livers of healthy mice. The fusion protein ZF-AS is catalytically active *in vitro*, stabilized in plasma, and traffics successfully and in fully intact form to the cytosol of cultured cells, achieving cytosolic concentrations greater than 100 nM. This value is 3−10-fold higher than the concentration of endogenous AS (11 ± 1 to 44 ± 5 nM). When injected into healthy C57BL/6 mice, ZF-AS reaches the mouse liver at concentrations almost 200 nM above baseline. These studies demonstrate that ZF5.3 can deliver a complex enzyme to the cytosol at therapeutically relevant concentrations and support its further development as an improved vehicle for cytosolic enzyme replacement therapies. These studies should also motivate efforts to establish more comprehensive design rules for endosomal escape[11] that are guided by directly and accurately quantifying delivery efficiency, not activity.

ASSOCIATED CONTENT

Supporting Information

The Supporting Information is available free of charge at https://pubs.acs.org/doi/10.1021/acscentsci.0c01603.

Methods, equipment, supplementary figures, supplementary tables, and additional information (PDF)

AUTHOR INFORMATION

Corresponding Author

Alanna Schepartz − *Department of Chemistry, University of California, Berkeley, California 94720, United States; Department of Molecular and Cell Biology and California Institute for Quantitative Biosciences, University of California, Berkeley, California 94720, United States;* orcid.org/0000-0003-2127-3932; Email: schepartz@berkeley.edu

Authors

Susan L. Knox − *Department of Chemistry, Yale University, New Haven, Connecticut 06511, United States; Department of Chemistry, University of California, Berkeley, California 94720, United States*

Rebecca Wissner − *Department of Chemistry, Yale University, New Haven, Connecticut 06511, United States*

Samantha Piszkiewicz − *Department of Chemistry, Yale University, New Haven, Connecticut 06511, United States; Department of Chemistry, University of California, Berkeley, California 94720, United States*

Complete contact information is available at: https://pubs.acs.org/10.1021/acscentsci.0c01603

Funding

This work was supported by the Blavatnik Fund for Innovation at Yale University. S.L.K. was supported by the National Institutes of Health (Chemistry-Biology Interface Training

Program (T32GM06754)) and the National Science Foundation Graduate Research Fellowship Program (DGE1752134). The QB3/Chemistry Mass Spectrometry Facility at UC Berkeley received NIH support (Grant 1S10OD020062-01).

Notes

The authors declare the following competing financial interest(s): A.S., S.L.K., R.W., and S.P. are named inventors of a pending patent application related to the work described.

■ ACKNOWLEDGMENTS

We are grateful to Charles River Laboratories for the large-scale preparation of AS and ZF-AS in ClearColi, *in vivo* mouse work, and liver homogenate studies; Dr. Matthew Wright at Genentech for guidance on evaluating liver delivery; Dr. Angela Steinauer for FCS training; and Dr. Joseph Wolenski for managing the Science Hill Imaging Facility at Yale University. We are also grateful to Susan Marqusee, Miriam Hood, and Eva Gerber for obtaining CD data and to Anthony Iavarone at QB3/Chemistry Mass Spectrometry Facility at UC Berkeley for mass spectrometry analysis of AS^{Rho} and ZF-AS^{Rho}.

■ REFERENCES

(1) Mullard, A. 2019 FDA Drug Approvals. *Nat. Rev. Drug Discovery* **2020**, *19* (2), 79−84.
(2) Dimitrov, D. S. Therapeutic Proteins. *Methods Mol. Biol.* **2012**, *899*, 1−26.
(3) Global pharmaceutical revenue by technology 2012−2026 https://www-statista-com.libproxy.berkeley.edu/statistics/309450/pharma-revenues-worldwide-prescription-drug-and-otc-by-technology/ (accessed Nov 7, 2020).
(4) Frankel, A. D.; Pabo, C. O. Cellular Uptake of the Tat Protein from Human Immunodeficiency Virus. *Cell* **1988**, *55* (6), 1189−1193.
(5) Green, M.; Loewenstein, P. M. Autonomous Functional Domains of Chemically Synthesized Human Immunodeficiency Virus Tat Trans-Activator Protein. *Cell* **1988**, *55* (6), 1179−1188.
(6) LeCher, J. C.; Nowak, S. J.; McMurry, J. L. Breaking in and Busting out: Cell-Penetrating Peptides and the Endosomal Escape Problem. *Biomol. Concepts* **2017**, *8* (3−4), 131−141.
(7) Bolhassani, A.; Jafarzade, B. S.; Mardani, G. In Vitro and in Vivo Delivery of Therapeutic Proteins Using Cell Penetrating Peptides. *Peptides* **2017**, *87*, 50−63.
(8) Steinauer, A.; LaRochelle, J. R.; Knox, S. L.; Wissner, R. F.; Berry, S.; Schepartz, A. HOPS-Dependent Endosomal Fusion Required for Efficient Cytosolic Delivery of Therapeutic Peptides and Small Proteins. *Proc. Natl. Acad. Sci. U. S. A.* **2019**, *116* (2), 512−521.
(9) Wissner, R. F.; Steinauer, A.; Knox, S. L.; Thompson, A. D.; Schepartz, A. Fluorescence Correlation Spectroscopy Reveals Efficient Cytosolic Delivery of Protein Cargo by Cell-Permeant Miniature Proteins. *ACS Cent. Sci.* **2018**, *4* (10), 1379−1393.
(10) Appelbaum, J. S.; LaRochelle, J. R.; Smith, B. A.; Balkin, D. M.; Holub, J. M.; Schepartz, A. Arginine Topology Controls Escape of Minimally Cationic Proteins from Early Endosomes to the Cytoplasm. *Chem. Biol.* **2012**, *19* (7), 819−830.
(11) LaRochelle, J. R.; Cobb, G. B.; Steinauer, A.; Rhoades, E.; Schepartz, A. Fluorescence Correlation Spectroscopy Reveals Highly Efficient Cytosolic Delivery of Certain Penta-Arg Proteins and Stapled Peptides. *J. Am. Chem. Soc.* **2015**, *137* (7), 2536−2541.
(12) Qian, Z.; Liu, T.; Liu, Y.-Y.; Briesewitz, R.; Barrios, A. M.; Jhiang, S. M.; Pei, D. Efficient Delivery of Cyclic Peptides into Mammalian Cells with Short Sequence Motifs. *ACS Chem. Biol.* **2013**, *8* (2), 423−431.
(13) Husson, A.; Brasse-Lagnel, C.; Fairand, A.; Renouf, S.; Lavoinne, A. Argininosuccinate Synthetase from the Urea Cycle to the Citrulline−NO Cycle. *Eur. J. Biochem.* **2003**, *270* (9), 1887−1899.
(14) Haines, R. J.; Pendleton, L. C.; Eichler, D. C. Argininosuccinate Synthase: At the Center of Arginine Metabolism. *Int. J. Biochem. Mol. Biol.* **2010**, *2* (1), 8−23.
(15) Diez-Fernandez, C.; Rüfenacht, V.; Häberle, J. Mutations in the Human Argininosuccinate Synthetase (ASS1) Gene, Impact on Patients, Common Changes, and Structural Considerations. *Hum. Mutat.* **2017**, *38* (5), 471−484.
(16) Kok, C. Y.; Cunningham, S. C.; Carpenter, K. H.; Dane, A. P.; Siew, S. M.; Logan, G. J.; Kuchel, P. W.; Alexander, I. E. Adeno-Associated Virus-Mediated Rescue of Neonatal Lethality in Argininosuccinate Synthetase-Deficient Mice. *Mol. Ther.* **2013**, *21* (10), 1823−1831.
(17) Herrera Sanchez, M. B.; Previdi, S.; Bruno, S.; Fonsato, V.; Deregibus, M. C.; Kholia, S.; Petrillo, S.; Tolosano, E.; Critelli, R.; Spada, M.; Romagnoli, R.; Salizzoni, M.; Tetta, C.; Camussi, G. Extracellular Vesicles from Human Liver Stem Cells Restore Argininosuccinate Synthase Deficiency. *Stem Cell Res. Ther.* **2017**, *8*, 176.
(18) Mingozzi, F.; High, K. A. Immune Responses to AAV Vectors: Overcoming Barriers to Successful Gene Therapy. *Blood* **2013**, *122* (1), 23−36.
(19) Masat, E.; Pavani, G.; Mingozzi, F. Humoral Immunity to AAV Vectors in Gene Therapy: Challenges and Potential Solutions. *Discovery Med.* **2013**, *15* (85), 379−389.
(20) Calcedo, R.; Wilson, J. Humoral Immune Response to AAV. *Front. Immunol.* **2013**, *4*, 341.
(21) Louis Jeune, V.; Joergensen, J. A.; Hajjar, R. J.; Weber, T. Pre-Existing Anti−Adeno-Associated Virus Antibodies as a Challenge in AAV Gene Therapy. *Hum. Gene Ther: Methods.* **2013**, *24* (2), 59−67.
(22) Naso, M. F.; Tomkowicz, B.; Perry, W. L.; Strohl, W. R. Adeno-Associated Virus (AAV) as a Vector for Gene Therapy. *Bio Drugs* **2017**, *31* (4), 317−334.
(23) Thomas, C. E.; Ehrhardt, A.; Kay, M. A. Progress and Problems with the Use of Viral Vectors for Gene Therapy. *Nat. Rev. Genet.* **2003**, *4* (5), 346−358.
(24) Hromada, C., Mühleder, S.; Grillari, J.; Redl, H.; Holnthoner, W. Endothelial Extracellular Vesicles—Promises and Challenges. *Front. Physiol.* **2017** *8* (275). DOI: 10.3389/fphys.2017.00275.
(25) Knox, S. L.; Steinauer, A.; Alpha-Cobb, G.; Trexler, A.; Rhoades, E.; Schepartz, A. Chapter Twenty-One - Quantification of Protein Delivery in Live Cells Using Fluorescence Correlation Spectroscopy. In *Methods in Enzymology*; Chenoweth, D. M., Ed.; Academic Press: 2020; Vol. *641*, pp 477−505. DOI: 10.1016/bs.mie.2020.05.007.
(26) Kuo, D.; Nie, M.; Courey, A. J. SUMO as a Solubility Tag and In Vivo Cleavage of SUMO Fusion Proteins with Ulp1. In *Protein Affinity Tags: Methods and Protocols*; Giannone, R. J., Dykstra, A. B., Eds.; Springer New York: New York, NY, 2014; pp 71−80. DOI: 10.1007/978-1-4939-1034-2_6.
(27) Karlberg, T.; Collins, R.; van den Berg, S.; Flores, A.; Hammarstrom, M.; Hogbom, M.; Holmberg Schiavone, L.; Uppenberg, J. Structure of Human Argininosuccinate Synthetase. *Acta Crystallogr., Sect. D: Biol. Crystallogr.* **2008**, *64* (3), 279−286.
(28) Diez-Fernandez, C.; Wellauer, O.; Gemperle, C.; Rüfenacht, V.; Fingerhut, R.; Häberle, J. Kinetic Mutations in Argininosuccinate Synthetase Deficiency: Characterisation and in Vitro Correction by Substrate Supplementation. *J. Med. Genet.* **2016**, *53* (10), 710.
(29) Theile, C. S.; Witte, M. D.; Blom, A. E. M.; Kundrat, L.; Ploegh, H. L.; Guimaraes, C. P. Site-Specific N-Terminal Labeling of Proteins Using Sortase-Mediated Reactions. *Nat. Protoc.* **2013**, *8* (9), 1800−1807.
(30) Guimaraes, C. P.; Witte, M. D.; Theile, C. S.; Bozkurt, G.; Kundrat, L.; Blom, A. E. M.; Ploegh, H. L. Site-Specific C-Terminal and Internal Loop Labeling of Proteins Using Sortase-Mediated Reactions. *Nat. Protoc.* **2013**, *8*, 1787.

(31) Popp, M. W.-L., Antos, J. M.; Ploegh, H. L. Site-Specific Protein Labeling via Sortase-Mediated Transpeptidation. *Curr. Protoc. Protein Sci.* **2009** *Chapter 15* Unit-15.3. DOI: 10.1002/0471140864.ps1503s56.
(32) Brusilow, S. W.; Horwich, A. L. Urea Cycle Enzymes. In *The Online Metabolic and Molecular Bases of Inherited Disease*; Beaudet, A. L., Vogelstein, B., Kinzler, K. W., Antonarakis, S. E., Ballabio, A., Gibson, K. M., Mitchell, G., Eds.; The McGraw-Hill Companies, Inc.: New York, NY, 2014.
(33) Saheki, T.; Sase, M.; Nakano, K.; Azuma, F.; Katsunuma, T. Some Properties of Argininosuccinate Synthetase Purified from Human Liver and a Comparison with the Rat Liver Enzyme. *J. Biochem.* **1983**, *93* (6), 1531−1537.
(34) Schimke, R. T. [38] Micromethods for the Assay of Argininosuccinate Synthetase, Argininosuccinase, and Arginase. In *Methods in Enzymology*; Academic Press: 1970; Vol. *17*, pp 324−329. DOI: 10.1016/0076-6879(71)17205-9.
(35) Wixom, R. L.; Reddy, M. K.; Cohen, P. P. A Concerted Response of the Enzymes of Urea Biosynthesis during Thyroxine-Induced Metamorphosis of Rana Catesbeiana. *J. Biol. Chem.* **1972**, *247* (11), 3684−3692.
(36) O'Brien, W. E. A Continuous Spectrophotometric Assay for Argininosuccinate Synthetase Based on Pyrophosphate Formation. *Anal. Biochem.* **1976**, *76* (2), 423−430.
(37) McMurry, J. L.; Chang, M. C. Y. Fluorothreonyl-TRNA Deacylase Prevents Mistranslation in the Organofluorine Producer Streptomyces Cattleya. *Proc. Natl. Acad. Sci. U. S. A.* **2017**, *114*, 11920.
(38) Ghose, C.; Raushel, F. M. Determination of the Mechanism of the Argininosuccinate Synthetase Reaction by Static and Dynamic Quench Experiments. *Biochemistry* **1985**, *24* (21), 5894−5898.
(39) Shaheen, N. K. Characterization of Human Wild-Type and Mutant Argininosuccinate Synthetase Proteins Expressed in Bacterial Cells. *Enzyme Protein* **2017**, *48*, 251−264.
(40) Berning, C.; Bieger, I.; Pauli, S.; Vermeulen, T.; Vogl, T.; Rummel, T.; Höhne, W.; Koch, H. G.; Rolinski, B.; Gempel, K.; Häberle, J. Investigation of Citrullinemia Type I Variants by in Vitro Expression Studies. *Hum. Mutat.* **2008**, *29* (10), 1222−1227.
(41) Kennaway, N. G.; Harwood, P. J.; Ramberg, D. A.; Koler, R. D.; Buist, N. R. M. Citrullinemia: Enzymatic Evidence for Genetic Heterogeneity. *Pediatr. Res.* **1975**, *9* (6), 554−558.
(42) Matsuda, Y., Tsuji, A.; Katunuma, N. Qualitative Abnormality of Liver Argininosuccinate Synthetase in a Patient with Citrullinemia. In *Urea Cycle Diseases*; Lowenthal, A., Mori, A., Marescau, B., Eds.; Springer US: Boston, MA, 1982; pp 77−82. DOI: 10.1007/978-1-4757-6903-6_10.
(43) Rochovansky, O.; Ratner, S. Biosynthesis of Urea: XII. FURTHER STUDIES ON ARGININOSUCCINATE SYNTHETASE: SUBSTRATE AFFINITY AND MECHANISM OF ACTION. *J. Biol. Chem.* **1967**, *242* (17), 3839−3849.
(44) Stanzl, E. G.; Trantow, B. M.; Vargas, J. R.; Wender, P. A. Fifteen Years of Cell-Penetrating, Guanidinium-Rich Molecular Transporters: Basic Science, Research Tools, and Clinical Applications. *Acc. Chem. Res.* **2013**, *46* (12), 2944−2954.
(45) Thompson, D. B.; Cronican, J. J.; Liu, D. R. Engineering and Identifying Supercharged Proteins for Macromolecule Delivery into Mammalian Cells. *Methods Enzymol.* **2012**, *503*, 293−319.
(46) McNaughton, B. R.; Cronican, J. J.; Thompson, D. B.; Liu, D. R. Mammalian Cell Penetration, SiRNA Transfection, and DNA Transfection by Supercharged Proteins. *Proc. Natl. Acad. Sci. U. S. A.* **2009**, *106* (15), 6111−6116.
(47) McAlpine, J. A.; Lu, H.-T.; Wu, K. C.; Knowles, S. K.; Thomson, J. A. Down-Regulation of Argininosuccinate Synthetase Is Associated with Cisplatin Resistance in Hepatocellular Carcinoma Cell Lines: Implications for PEGylated Arginine Deiminase Combination Therapy. *BMC Cancer* **2014**, *14* (1), 621.
(48) Holub, J. M.; LaRochelle, J. R.; Appelbaum, J. S.; Schepartz, A. Improved Assays for Determining the Cytosolic Access of Peptides, Proteins, and Their Mimetics. *Biochemistry* **2013**, *52* (50), 9036−9046.
(49) Raetz, C. R. H.; Whitfield, C. Lipopolysaccharide Endotoxins. *Annu. Rev. Biochem.* **2002**, *71* (1), 635−700.
(50) Schmidt, F. R. Recombinant Expression Systems in the Pharmaceutical Industry. *Appl. Microbiol. Biotechnol.* **2004**, *65* (4), 363−372.
(51) Sandle, T. Removal of Endotoxin from Protein in Pharmaceutical Processes. *Am. Pharm. Rev.* **2016**, *19*, 1−5.
(52) Dullah, E. C.; Ongkudon, C. M. Current Trends in Endotoxin Detection and Analysis of Endotoxin−Protein Interactions. *Crit. Rev. Biotechnol.* **2017**, *37* (2), 251−261.
(53) Mamat, U.; Wilke, K.; Bramhill, D.; Schromm, A. B.; Lindner, B.; Kohl, T. A.; Corchero, J. L.; Villaverde, A.; Schaffer, L.; Head, S. R.; Souvignier, C.; Meredith, T. C.; Woodard, R. W. Detoxifying Escherichia Coli for Endotoxin-Free Production of Recombinant Proteins. *Microb. Cell Fact.* **2015**, *14* (1), 57.
(54) Morrison, D. C.; Ryan, J. L. Bacterial Endotoxins and Host Immune Responses. In *Advances in Immunology*; Dixon, F. J., Kunkel, H. G., Eds.; Academic Press, 1980; Vol. *28*, pp 293−450. DOI: 10.1016/S0065-2776(08)60802-0.
(55) Teghanemt, A.; Zhang, D.; Levis, E. N.; Weiss, J. P.; Gioannini, T. L. Molecular Basis of Reduced Potency of Underacylated Endotoxins. *J. Immunol.* **2005**, *175* (7), 4669.
(56) Saitoh, S.; Akashi, S.; Yamada, T.; Tanimura, N.; Kobayashi, M.; Konno, K.; Matsumoto, F.; Fukase, K.; Kusumoto, S.; Nagai, Y.; Kusumoto, Y.; Kosugi, A.; Miyake, K. Lipid A Antagonist, Lipid IVa, Is Distinct from Lipid A in Interaction with Toll-like Receptor 4 (TLR4)-MD-2 and Ligand-induced TLR4 Oligomerization. *Int. Immunol.* **2004**, *16* (7), 961−969.
(57) Satoh, M.; Iwahori, T.; Sugawara, N.; Yamazaki, M. Liver Argininosuccinate Synthase Binds to Bacterial Lipopolysaccharides and Lipid A and Inactivates Their Biological Activities. *J. Endotoxin Res.* **2006**, *12* (1), 21−38.
(58) USP. Chapter 85, Bacterial Endotoxins Test. 2011.
(59) Dawson, M. Endotoxin Limits for Parenteral Drug Products. *BET White Paper* 2017.
(60) *Guidance for Industry Pyrogen and Endotoxins Testing: Questions and Answers*. U.S. Department of Health and Human Services 2012.
(61) Tsuji, K.; Steindler, K. A.; Harrison, S. J. Limulus Amoebocyte Lysate Assay for Detection and Quantitation of Endotoxin in a Small-Volume Parenteral Product. *Appl. Environ. Microbiol.* **1980**, *40* (3), 533−538.
(62) Rueda, F.; Cano-Garrido, O.; Mamat, U.; Wilke, K.; Seras-Franzoso, J.; García-Fruitós, E.; Villaverde, A. Production of Functional Inclusion Bodies in Endotoxin-Free Escherichia Coli. *Appl. Microbiol. Biotechnol.* **2014**, *98* (22), 9229−9238.
(63) Coats, S. R.; Pham, T.-T. T.; Bainbridge, B. W.; Reife, R. A.; Darveau, R. P. MD-2 Mediates the Ability of Tetra-Acylated and Penta-Acylated Lipopolysaccharides to Antagonize Escherichia Coli Lipopolysaccharide at the TLR4 Signaling Complex. *J. Immunol.* **2005**, *175* (7), 4490.
(64) Visintin, A.; Halmen, K. A.; Latz, E.; Monks, B. G.; Golenbock, D. T. Pharmacological Inhibition of Endotoxin Responses Is Achieved by Targeting the TLR4 Coreceptor, MD-2. *J. Immunol.* **2005**, *175* (10), 6465.
(65) Saheki, T.; Komorizono, K.; Miura, T.; Ichiki, H.; Yagi, Y.; Hashimoto, S. Clearance of Argininosuccinate Synthetase from the Circulation in Acute Liver Disease. *Clin. Biochem.* **1990**, *23* (2), 139−141.
(66) Perez, C. J.; Jaubert, J.; Guénet, J.-L.; Barnhart, K. F.; Ross-Inta, C. M.; Quintanilla, V. C.; Aubin, I.; Brandon, J. L.; Otto, N. W.; DiGiovanni, J.; Gimenez-Conti, I.; Giulivi, C.; Kusewitt, D. F.; Conti, C. J.; Benavides, F. Two Hypomorphic Alleles of Mouse Ass1 as a New Animal Model of Citrullinemia Type I and Other Hyperammonemic Syndromes. *Am. J. Pathol.* **2010**, *177* (4), 1958−1968.